Understanding Aortic Dissection Hemodynamics: Evaluating Adapted Smoke Surfaces Against Streakline-Based Techniques

Aaron Schroeder, Kai Ostendorf, Kathrin Bäumler, Domenico Mastrodicasa, Dominik Fleischmann, Bernhard Preim, Holger Theisel, and Gabriel Mistelbauer

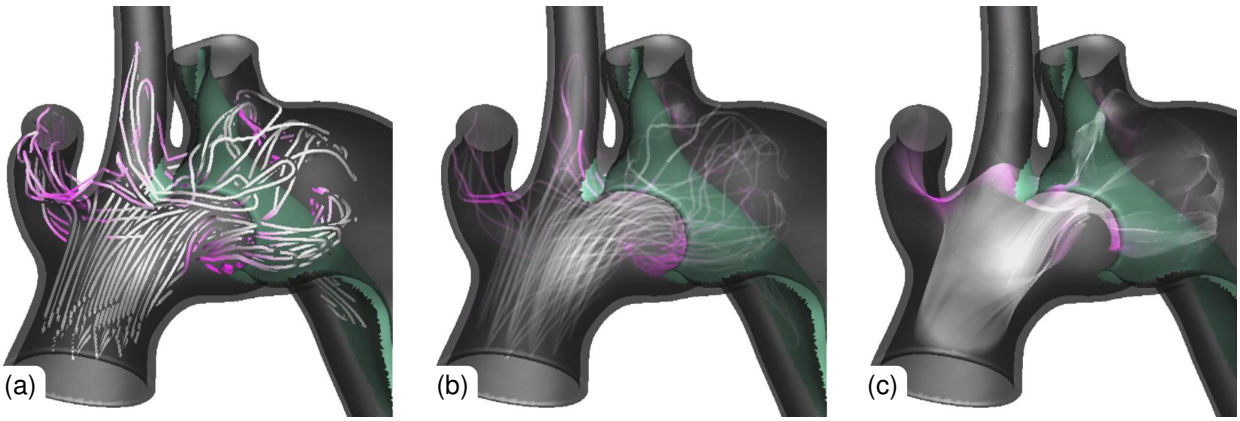

Fig. 1: Freeze frame from an evaluation video showing flow at the aortic root, into branches, and through the entry tear. Streaklines with halos (a), transparent streaklines (b), and smoke surfaces (c) use flow-direction color mapping: white for antegrade, magenta for retrograde. Seeding location, structure length, color mapping, and viewing direction are synchronized.

Abstract—Aortic dissection is a life-threatening cardiovascular disease characterized by blood entering the media layer of the aortic vessel wall. This creates a second flow channel, known as the false lumen, which weakens the aortic wall and can potentially lead to fatal aortic rupture. Current risk stratification of aortic dissections is primarily based on morphological features of the aorta. However, hemodynamics also play a significant role in disease progression, though their investigation and visualization remain challenging. Common flow visualizations often experience visual clutter, especially when dealing with the intricate morphologies of aortic dissections. In this work, we implement and evaluate different approaches to visualizing the flow in aortic dissections effectively. We employ three techniques, namely streaklines with depth-dependent halos, transparent streaklines, and smoke surfaces. The latter is a technique based on streak surfaces, enhanced with opacity modulations, to produce a smoke-like appearance that improves visual clarity. We adapt the original opacity modulation of smoke surfaces to visualize flow even within the complex geometries of aortic dissections, thereby enhancing visual fidelity. To effectively capture dissection hemodynamics, we developed customized seeding structures that adapt to the shape of the surrounding lumen. Our evaluation, conducted via an online questionnaire, included medical professionals, fluid simulation experts, and visualization specialists. By analyzing results across these groups, we highlight differences in preference and interpretability, offering insight into domain-specific needs. No single visualization technique emerged as the best overall. Smoke surfaces provide the best overall clarity and visual realism. However, participants found streaklines with halos to be the best for quantifying flow, dispite them introducing significant visual clutter. Transparent streaklines serve as a middle ground, offering improved clarity over halos while maintaining some level of detail. Across all participant groups, smoke surfaces were rated as the most visually appealing and lifelike, with medical professionals highlighting their resemblance to contrast-agent injections used in clinical practice.

Index Terms—Medical Visualization, Flow Visualization, Hemodynamics, Aortic Dissection.

1 Introduction

Aortic dissection is a rare but life-threatening cardiovascular disease [1, 2]. Patients require continuous clinical monitoring to prevent complications such as branch vessel malperfusion, or aortic rupture [3].

- *Aaron Schroeder, Kai Ostendorf, Bernhard Preim, and Holger Theisel are with Otto-von-Guericke-University, Magdeburg, Germany. E-mail: aaron.schroeder, kai.ostendorf, bernhard.preim, holger.theisel@ovgu.de.*
- *Kathrin Bäumler, Dominik Fleischmann, and Gabriel Mistelbauer are with Stanford University: Stanford, CA, US. E-mail: baeumler, d.fleischmann, gmistelb@stanford.edu.*
- *Domenico Mastrodicasa is with University of Washington: Seattle, Washington, US. E-mail: mastrodm@uw.edu.*

Manuscript received xx xxx. 201x; accepted xx xxx. 201x. Date of Publication xx xxx. 201x; date of current version xx xxx. 201x. For information on obtaining reprints of this article, please send e-mail to: reprints@ieee.org. Digital Object Identifier: xx.xxxx/TVCG.201x.xxxxxxx

Aortic dissection occurs when blood enters the media layer of the aortic vessel wall, creating a secondary flow channel called the false lumen, which runs parallel to the original flow channel, known as the true lumen. A thin membrane, the dissection flap, separates the true and false lumina; this flap is the delaminated portion of the aortic vessel wall. The extent of the false lumen can vary significantly between patients. The dissection typically begins at the original entry site, called the entry tear. It extends along the aorta, and may end at one or more exit tears distal to the entry tear. Furthermore, additional tears, known as fenestrations, may be present. Analyzing the anatomy and hemodynamics of aortic dissections is challenging due to the considerable variability in their configurations.

Currently, the classification, treatment, and prognosis of aortic dissection are primarily informed by morphological features [4]. Studies suggest that true lumen collapse and branch vessel malperfusion are related to the number, size, and location of intimal tears, as well as the distribution of branch vessels draining the false and true lu-

men [5, 6]. Increased false lumen pressure may also relate to false lumen dilation [7, 8], which can culminate in aortic rupture. Limited false lumen outflow, on the other hand, contributes to overall disease progression [9, 10]. These findings demonstrate that the hemodynamics of aortic dissection significantly impact disease progression.

Previous techniques for visualizing aortic dissection hemodynamics have predominantly relied on line-based methods [11]. These approaches frequently suffer from severe visual clutter and occlusion due to the extensive overlapping of numerous lines. Methods aimed at reducing this clutter, by either limiting the number of lines or enhancing their depth perception, restrict the exploratory analysis of hemodynamics. Consequently, effective visualization of complex hemodynamic data, such as that associated with aortic dissections, requires specialized flow visualization techniques.

Virtual flow visualization is fundamentally inspired by real-life experimental flow visualization methods, which typically involve introducing a medium such as smoke or dye into flow and observing its advection. This methodology is also applied in contrast-enhanced angiography, where contrast agent is administered into the bloodstream to highlight vessels in medical imaging data. Contrast agent is injected at a single site and dissipates through the vascular system as it is advected by flow. Although contrast agents in fluids and smoke in gases are governed by slightly different physical principles, they exhibit comparable visual characteristics:

- fine-scale local seeding structures,
- opacity correlated with agent concentration, and
- exponential attenuation of opacity with increasing medium thickness.

These parallels inspired our adaptation of a smoke visualization technique. Specifically, we employ smoke surfaces [12], a method derived from streak surfaces, for the visualization of aortic blood flow. Building on previous work by Schroeder et al. [11], which introduced tailored visualizations for aortic dissection flow, we developed advanced techniques to enhance the depiction of complex hemodynamics in aortic dissections, aiming to improve clarity and reduce visual clutter. To mitigate clutter and occlusion caused by dense seeding, we apply smoke surfaces and augment the technique introduced by Funck et al. with opacity modulations that reduce artifacts resulting from the unique structure of aortic dissection. Our major technical contributions are:

- an interactive exploration of hemodynamics and vascular morphology
- a customized seeding strategy to enhance flow visualization in complex vascular structures, and
- a tailored opacity and rendering technique to reduce visual clutter while preserving critical flow details.

While these contributions address some of the challenges in hemodynamic visualization, it remains unclear which technique is most suitable for specific use cases (UCs), different regions along the aorta, and various user groups such as medical professionals, computational fluid dynamics (CFD) simulation experts, and visualization specialists. The effectiveness of different visualization methods may vary depending on the specific requirements and expertise of the user, as well as the particular area of interest within the aortic structure.

To address this gap and provide initial insights, we conducted a comparative analysis of three major flow visualization techniques: streaklines with depth-dependent halos, transparent streaklines, and our adapted smoke surfaces. This evaluation aims to explore the strengths and limitations of each approach in various scenarios and user groups.

We aim to provide initial guidance and generate hypotheses on the suitability of visualization techniques for specific clinical and research applications in aortic dissection analysis. This approach not only enhances our understanding of flow visualization techniques but also lays the groundwork for more extensive future studies bridging theoretical advancements and practical implementation in both medical and research settings.

The remainder of this paper is structured as follows: Section 2 discusses related work. Section 3 details our methodology, including data processing, visualization techniques, augmentation of smoke surfaces, seeding structures, and color mapping. Section 4 outlines our evaluation design, followed by Section 5, which presents the results and a comprehensive discussion. Finally, Section 6 concludes the paper and suggests directions for future work.

2 Related Work

Flow visualization techniques are increasingly used in a medical setting, particularly in diagnosing and treating cardiovascular diseases [13]. They are mostly based on either magnetic resonance imaging (MRI) measurements or CFD simulations [14]. Specialized techniques for flow visualization of specific vascular structures such as the aorta [15] or carotid arteries [16] and specific diseases such as aneurysms [17, 18] were presented.

Little work has been done on techniques tailored to the visualization of the anatomy and blood flow within aortic dissections. Ostendorf et al. [19] assessed shading styles for the rendering of multiple vessel wall surfaces, specifically the outer vessel wall and dissection flap. We use their findings to render the aortic vessel wall and dissection flap. Schroeder et al. [11] recently presented a visualization system tailored to the complex flow associated with aortic dissection. They used pathlines with color coding of hemodynamic information to show flow, combined with rendering of the outer vessel wall and the dissection flap. We are extending this work, by using a smoke-like visualization of flow, to reduce clutter and improve the appearance of the flow visualization.

2.1 Smoke-like Flow Visualization

The depictions of flow using techniques inspired by experimental flow visualization can aid in the intuitive understanding of complex flow dynamics and the interpretability of those visualizations. Line-based flow visualization techniques do not lend themselves well to creating a smoke-like appearance.

2.1.1 Particle-based Techniques

To enhance the appearance of smoke while minimizing the number of particles needed for a convincing effect, various techniques have been developed. These include surface-particles [20], rendered as points with normals, semi-transparent billboards [21], and point sprites [22]. Aiming to simulate the injection of particles into the blood flow, De Hoon et al. [23] created flow visualizations of aortic flow based on phase-contrast MRI data. A smoke-like appearance was achieved by advecting numerous particles and rendering them semi-transparently. Color mapping was applied to the particles, which encoded seeding position or particle age but no hemodynamic properties.

2.1.2 Streak Surface Techniques

Stream surfaces have been used extensively in flow visualization [24–27]. Unlike stream and path surfaces, streak surfaces require periodic emission and simultaneous advection of vertices, making structural changes possible anywhere on the surface. This necessitates constant checks, historically limiting their use in interactive applications.

Von Funck et al. [12] introduced *Smoke Surfaces*, which avoid restructuring by using opacity modulation to simulate smoke. Their method balances realism and computational efficiency, hiding overly deformed mesh cells and enabling interactive visualization. We adapt their method for the visualization of aortic dissection flow, as detailed in Section 4.2. Shortly after, Bürger et al. [28] enabled interactive streak surface visualizations with proper mesh restructuring. Ferstl et al. [29] then adapted their patch-based approach for interactive separating streak surfaces. Hummel et al. [30] introduced an illustrative rendering approach for stream, path, and streak surfaces, compatible with interactive visualization without requiring expensive preprocessing. Recently, Schindler et al. [31] applied the technique of von Funck et al. [12] to animated streak surfaces. They use smoke surfaces for the comparison of multiple trajectories emerging from different initial conditions of a 4D biological dynamical system.

2.1.3 Volumetric Techniques

Interactive visualizations of gaseous phenomena became possible with volumetric approaches, where ray casting replaces geometric rendering. This technique is common in medical imaging, as MRI and computed tomography (CT) directly provide volumetric data. Schpok et al. [32] pioneered realistic animated cloud rendering, followed by Zhou et al. [33], who introduced interactive smoke rendering with dynamic lighting using compensated ray marching. In flow visualization, flow volumes [34] emerged as the volumetric counterpart to streamlines, forming integral volumes by advecting meshes instead of individual seed points. The resulting segments are subdivided into tetrahedra and rendered via volume rendering.

2.2 Advection Performance

Cell localization and data access are crucial for achieving interactive frame rates, especially for live advection. While structured data typically enables quick cell localization, unstructured data requires specialized techniques for efficient access. Most medical flow data, such as MRI scans, come in structured grids, enabling easy GPU use and constant-time cell localization, as shown by De Hoon et al. [23]. For unstructured data, hierarchical structures like octrees [35, 36] or kd-trees can speed up cell localization. Andrysco and Tricoche [37] addressed kd-trees' memory overhead with an efficient storage scheme. Yenpure et al. [38] review state-of-the-art techniques for improving particle advection performance in flow visualizations. We employ a two-level structure to improve data access, as described in Section 4.1.

3 Visualization Task Analysis

Schroeder et al. [11] identified three UCs that encapsulate the complex hemodynamics inherent to aortic dissection. Each UC focuses on a distinct aspect of the disease, requiring specialized anatomical and functional visualization techniques.

The following sections provide brief descriptions of the tasks associated with each UC, including their motivation, background, intended target users, and expected benefits. UC 2 is not covered in detail in this work, as it focuses on dissection flap deformation and vessel wall properties rather than flow visualizations in the fluid domain (blood). For a more detailed task and requirement analysis, please see Schroeder et al. [11].

Use Case 1: Visualization of True and False Lumen Blood Flow in Aortic Dissection Hemodynamic visualizations assist CFD simulation experts in understanding the interaction between morphology and blood flow, helping to develop hypotheses on how flow dynamics contribute to late adverse events. In cardiothoracic and vascular surgery, these visualizations support the development of initial treatment strategies and precise device placement by providing a clear representation of the complex interplay between morphology and hemodynamics. Additionally, they aid surgeons in executing treatment approaches by simplifying otherwise intricate structural patterns. UC 1 encompasses the following visualization tasks:

- (T1) Visualizing blood flow
- (T2) Highlighting slow and fast flow
- (T3) Identifying retrograde flow
- (T4) Visualizing drainage pattern

Use Case 3: Effect of Dissection-Specific Blood Flow on the False Lumen Outer Wall False lumen pressurization may result from multiple factors. Patient-specific CFD simulations suggest that dissection flap mobility can alleviate pressure [39]. Surgical interventions, such as creating a distal fenestration, aim to decompress a hypertensive false lumen [40]. Visualizing blood flow through these communications could help assess treatment effectiveness. When blood enters another lumen through an entry tear or fenestration, it accelerates, forming a flow jet. The first task of UC 3 is to visualize these flow jets (T5). However, analyzing only the flow through a fenestration may be insufficient, as the jet may impact the opposing vessel wall, creating a so-called impingement zone. Understanding these zones, where morphology and hemodynamics interact, is essential. Thus, the second task of this UC is to identify and emphasize impingement zones (T6). For radiologists and surgeons, it is crucial to determine whether luminal communications significantly affect inflow or outflow. Closing a hemodynamically significant communication could have unintended consequences, such as false lumen expansion.

Application to This Work The visualization tasks identified in Schroeder et al.'s work remain relevant for comprehensive visualization of aortic dissection flow [11]. Therefore, we used them as a baseline to select and design the flow visualization techniques compared in this study. All tasks from UC 1 and UC 3 are addressed by streaklines with halos, transparent streaklines, and smoke surfaces.

4 Methods

Smoke surfaces are continuous streak surfaces with opacity modulation that produce a smoke-like appearance [12]. To evaluate smoke surfaces for the visualization of aortic flow, we compare them to two commonly used streakline-based techniques: streaklines with depth-dependent halos [41] and transparent streaklines.

In addition to the flow visualization, we display the outer vessel wall and the dissection flap without obstructing the display of flow. The vessel wall is rendered semi-transparently with a Fresnel effect [42], allowing internal structures to be seen while enabling assessment of the vessel's shape. The dissection flap is rendered opaque to avoid excessive transparent layers and to emphasize its shape and curvature. Hemodynamic and derived measures can be visually mapped onto these surfaces to depict wall motion, flow advection, and contrast agent dissipation, all integrated into a single visualization. All aspects of our visualization, including dissection morphology display, flow visualization, and color mappings, were developed in close collaboration with cardiovascular imaging scientists, radiologists, and clinicians experienced in aortic dissection treatment, some of whom are coauthors.

4.1 Input Data

Bäumler et al. [3] created high-resolution flow simulations of aortic dissections using computed tomography angiography (CTA) and 4D Flow MRI data from patients and phantom models and validated these simulations by comparing them to 4D Flow MRI measurements of the same morphology; these simulations serve as input for our visualizations. CTA data were used to segment the aorta, enabling the extraction of the vessel wall, blood volume, and dissection flap. The flow field from 4D Flow MRI provided information on flow velocity at various locations (e.g., aortic root, branching vessels). Blood flow and vessel tissue deformation were then simulated using two-way fluid-structure interaction CFD simulations, spanning multiple cardiac cycles with 4000 steps per cycle. The final cardiac cycle was recorded every 50th step, yielding 80 timesteps, 40 of which were used to balance temporal resolution, computational cost, and memory usage. The simulation results included two separate, unstructured tetrahedral meshes: the fluid volume and the vessel tissue, including the outer vessel wall and dissection flap. These meshes contain multiple hemodynamic and mechanical measurements, such as pressure, wall shear stress (WSS), displacement, position, and velocity.

Interactive advection of hundreds of points inside a fluid requires fast access to flow data. Due to the unstructured nature of the simulated data, integration is computationally expensive. To mitigate this issue and improve access times, we convert the simulation data to a regular grid data structure.

Vector fields can be organized to satisfy specific requirements for acquisition, simulation, and visualization [38]. Regular grids with uniform spacing along each axis are commonly used, as they offer consistent spatial sampling and allow for fast access. We resample the tetrahedral mesh data from the CFD simulations to a regular rectilinear grid with isotropic spacing. All values such as velocity vectors, pressure, and WSS are linearly interpolated, transferring the simulation results into a structured grid. This approach also improves compatibility with MRI datasets since their voxel data structure is very similar.

Due to the deformable vessel wall used during simulation, all vertices of the mesh move over the course of a cardiac cycle. When converting to a structured grid, the same tetrahedron cell can end up in

different voxels of the structured grid depending on its position, which changes over time. Consequently, each timestep must be converted to a structured grid individually while maintaining the same bounding box and voxel size. Finally, all converted timesteps are concatenated.

To reduce the memory consumption of the voxelized flow data, we convert it into a sparse representation. This data structure—similar to a two-level octree—eliminates data regions that remain empty across all time steps. Because the empty regions are consistent over time, only a single registry is needed to store the memory locations of non-empty regions. At the same time, constant-time access to the data is retained.

4.2 Smoke Surfaces

When using streak surfaces for visualization, individually advected vertices can move together or spread apart, compromising the structure of the streak surface mesh. To address this, vertex spacing must be monitored during each advection step to determine where vertices should be inserted or merged. Inserting a vertex requires placing it at the seeding location and advecting it to match the mesh's advection time, a process that can occur at multiple points simultaneously. Subsequently, the mesh must be re-triangulated to incorporate new vertices and maintain high-quality triangles. This process is computationally expensive, hindering interactive streak surface visualization.

Von Funck et al. [12] avoid mesh modifications by retaining consistent connectivity between vertices of the mesh and modulating the opacity of severely deformed triangle cells. Since the mesh connectivity is established only once, there is no need for re-triangulation. Multiple opacity factors contribute to a smoke-like appearance, helping to avoid artifacts from the compromised structure of the streak surface mesh. The vertex opacity for each triangle is calculated as follows:

$$\alpha = \alpha_{\text{density}} \cdot \alpha_{\text{shape}} \cdot \alpha_{\text{curvature}} \cdot \alpha_{\text{fade}}, \tag{1}$$

where α is the opacity value assigned to each vertex, α_{density} simulates smoke density, and α_{shape} equals 1.0 for equilateral triangles and decreases as the triangle deforms. This controls the opacity based on triangle quality. The opacity of the smoke surface is reduced by $\alpha_{\text{curvature}}$ as curvature increases. Finally, α_{fade} steadily decreases the opacity of vertices as they are advected, simulating smoke dispersion.

Smoke surfaces [12], originally tested on aerodynamic datasets, face challenges when applied to vascular structures like aortic dissections: When the flow splits between the true and false lumen, vertices advected into the false lumen remain erroneously connected to those in the true lumen. This incorrect connectivity suggests flow through the dissection flap that physically separates the two flow channels. The original opacity terms failed to adequately hide these false connections, which tend to be thin and stretch across the flap. These **surfaces intersecting the flap** can be observed in Figure 2a and Figure 2c. To address this issue, we have adapted key aspects of the opacity calculations.

4.3 Surfaces Intersecting the Flap

To address parts of the smoke surface mesh intersecting the flap, we introduce a per-triangle measurement of the longest edge length, $d_{\max}$. We raise the original shape opacity term to the power of $d_{\max}$, significantly reducing the opacity of elongated cells. A lower limit of $d_{\max} = 1$ ensures opacity is not unintentionally increased for short cells. Initially, the shape opacity term was calculated as follows:

$$\alpha_{\text{shape}}^{\text{original}} = \left(\frac{4\, area\,(\mathbf{x}_0, \mathbf{x}_1, \mathbf{x}_2)}{\sqrt{3}\, \max\{d_0 d_1, d_1 d_2, d_2 d_0\}} \right)^s, \tag{2}$$

where $\mathbf{x}_0, \mathbf{x}_1, \mathbf{x}_2$ are the three vertices of a triangle, d_0, d_1, d_2 are the triangle's edge lengths, and s controls the impact of α_{shape} on the final opacity. In contrast, our updated α_{shape} calculation, which includes the longest edge length $d_{\max}$, is:

$$\begin{aligned} d_{\max} &= \max\,(d_0, d_1, d_2)\,, \\ \alpha_{\text{shape}} &= \left(\left(\frac{4\, area\,(\mathbf{x}_0, \mathbf{x}_1, \mathbf{x}_2)}{\sqrt{3}\, \max\{d_0 d_1, d_1 d_2, d_2 d_0\}} \right)^{\max(1, d_{\max})} \right)^s. \end{aligned} \tag{3}$$

As a result of this modification, surfaces intersecting the flap are effectively hidden (Figure 2b and Figure 2d).

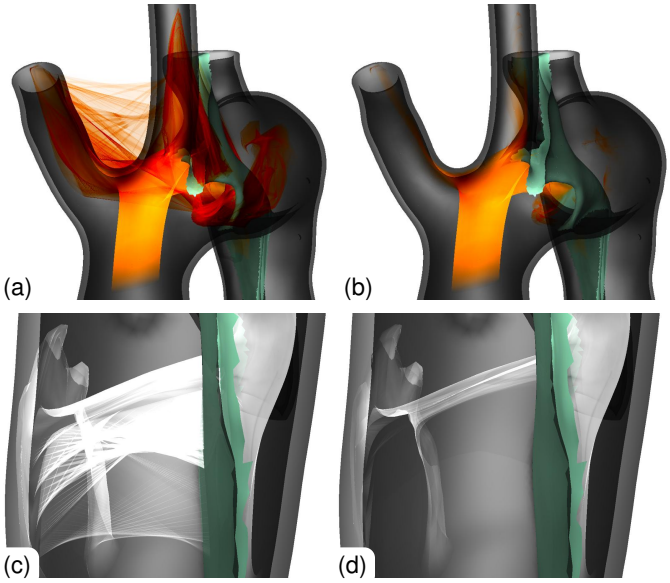

Fig. 2: Comparison of original and improved shape opacity terms. (a, b) show streak surfaces seeded in the ascending aorta that extend into arch branches and both lumina of the descending aorta. (c, d) show surfaces seeded near a fenestration in the descending aorta. The left column (a, c) uses the original α_{shape}, while the right column (b, d) applies the improved formulation.

4.4 Streaklines

To compare smoke surfaces with more commonly used flow visualization techniques, we selected two representative methods based on streaklines. The streakline visualization techniques are not part of this work, but serve as an example of commonly used hemodynamic visualization techniques. A streakline is formed by tracing individual fluid particles that pass through a fixed point in the flow and connecting them to form a line. This results in a visualization of flow similar to injecting a thin stream of smoke into an airflow. Despite the wide usage of this technique, it has several limitations. Enabling the analysis of a significant part of the flow requires multiple streaklines, which quickly leads to visual clutter and occlusion. We enhance their appearance by applying two different augmentation techniques to the streaklines.

Depth-dependent Halos The first technique, depth-dependent halos, was introduced by Everts et al. [41] to reduce visual clutter by selectively obscuring background lines. In this approach, an additional set of surfaces is generated behind each streakline, extending beyond the line itself to form a halo. These halos not only occlude lines in the background but also reduce clutter caused by numerous small line segments. This method improves clarity while increasing occlusion. Streaklines with halos are shown in Figure 1a.

Transparent Streaklines The second streakline augmentation, transparent streaklines, takes the opposite approach to depth-dependent halos by enhancing background visibility through transparency rather than occlusion. Opacity gradually decreases along the length of the streakline, starting from the seeding location, which helps convey flow direction. Additionally, a short lead-in fade is applied at the seed point to create a smoother transition and improve visual clarity. Transparent streaklines are shown in Figure 1b.

4.5 Seeding Structure

Effective seeding is fundamental for accurately visualizing flow behavior, as it directly influences the distribution and clarity of the generated structures. In the context of vascular flow, careful placement of seed points ensures interpretable visualizations. We distinguish between two primary approaches: grid seeding and adaptive circular seeding.

4.5.1 Grid Seeding

For the seeding of streak lines, we use the grid approach from Schroeder et al. [11]. We generate evenly spaced seed points covering the cross-sectional area of a lumen. A dense set of seed points is generated by placing points on concentric circles around the center of the cross-section. Even spacing between points on the same circle and between consecutive circles ensures a uniform distribution of points.

4.5.2 Adaptive Circular Seeding

Von Funck et al. [12] used a polygonal seeding structure $(\mathbf{s}_0, \ldots, \mathbf{s}_{N-1})$ composed of N equidistant seed points $\mathbf{s}_j$ along a continuous line or curve. This allows for flexible positioning and extent of the surface. To maintain connectivity and create a closed surface during advection, the smoke surface is designed with cylindrical topology. In the vertex array $\mathbf{x}_{i,j}$ (with $i \in [0, M[$ and $j \in [0, N[$), the vertices in the first column $(\mathbf{x}_{0,0}, \ldots, \mathbf{x}_{0,N-1})$ are connected to those in the last column $(\mathbf{x}_{M-1,0}, \ldots, \mathbf{x}_{M-1,N-1})$. M refers to the number of columns of vertices emitted from the seed points.

Continuous curve seeding structures work well for visualizing flow around airfoils and car bodies [12]. To visualize vascular hemodynamics, however, placement of curve seeding structures is challenging due to complex morphology, which often results in poor coverage of relevant flow features or oversampling of others. Therefore, aortic dissections require specialized seeding structures that can be adjusted quickly to support exploration and provide precise, uniform seeding.

We modified von Funck et al.'s method [12] by closing the curve to form a ring, replicating vascular morphology and generating a closed, tubular smoke surface. In addition to connecting the first and last columns of the mesh, we connect the first $(\mathbf{x}_{0,0}, \ldots, \mathbf{x}_{M-1,0})$ and last $(\mathbf{x}_{0,N-1}, \ldots, \mathbf{x}_{M-1,N-1})$ rows. The resulting smoke surface mesh forms a closed surface with toroidal topology.

To accommodate the distinct geometry of aortic dissections, we create a seeding structure based on the cross-section of the surrounding lumen, resulting in a roughly circular polygon of evenly spaced points that adapt to the vessel's shape. The user can adjust the distance between seed points and the vessel wall, with all points placed at the same relative position between the wall and cross-section center. This method yields an approximately circular seeding structure at smaller sizes, with seed points situated around the center. As the size increases, the seeding structure progressively conforms to the lumen shape (Figure 3).

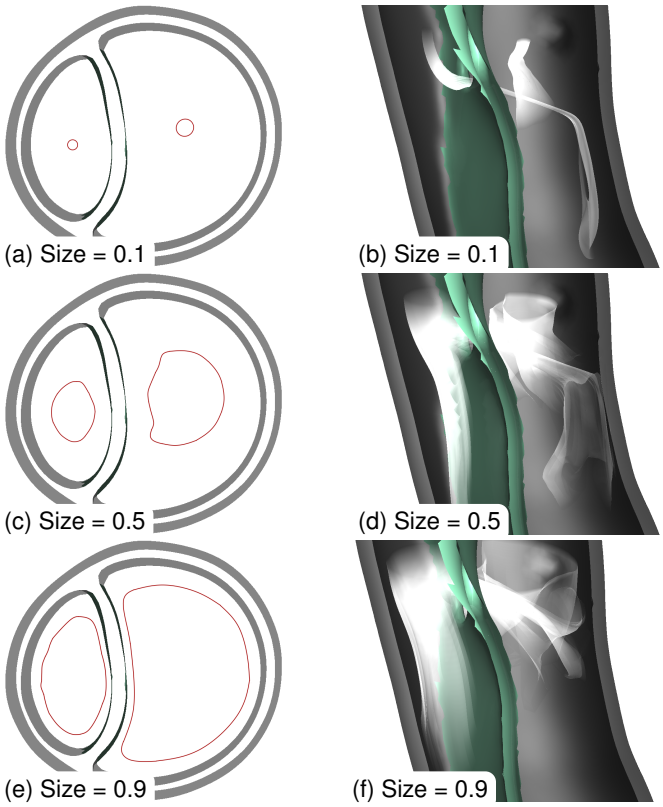

Fig. 3: Adaptive circular seeding in a cross-section of an aortic dissection. Each example shows a streak surface (white), outer wall (gray), and dissection flap (green). Seed point distances from center: 0.1 (a,b), 0.5 (c,d), and 0.9 (e,f), demonstrating adaptation to lumen shape. Left: cross-section with seeding (red). Right: side view showing resulting smoke surfaces.

4.6 Color Mapping

Color mapping enhances the interpretability of smoke surfaces by visually encoding various flow parameters. We use the same color mappings introduced by Schroeder et al. [11] for flow velocity, flow direction, and lumen-of-origin, with only slight adjustments to the color scheme. These mappings provide intuitive insights into complex flow dynamics. When no property is mapped to the flow visualization, we use a solid white color.

Flow velocity is visualized using a heated-body color scale, ranging from black (minimum) to bright yellow (maximum), which helps to distinguish phenomena like flow jets and stagnant flow. Lumen-of-origin is depicted with a diverging color scale, transitioning from red (true lumen) through white (transition) to blue (false lumen), effectively illustrating flow interactions and transitions between different lumina. Flow direction is mapped using a white-to-magenta monochrome scale, where white represents normal antegrade flow and magenta highlights retrograde flow.

4.7 Implementation

Streak surface advection is well-suited for parallelization since each surface mesh vertex can be processed independently. Smoke surface generation and animation require not only vertex advection but also per-frame parameter updates. To ensure interactive frame rates, we use compute shaders in Vulkan [43]. Our approach involves three compute shaders: one for vertex advection, one for per-face parameter and normal computation, and one for per-vertex parameter and normal computation. The final parameters are combined upon ray intersection using Vulkan's closest-hit shader.

The **advection shader** updates vertex positions by sampling, integrating, and interpolating the vector field. Proper advection depends on the mesh size (rows and columns) and the time difference between columns (t_{col}), which controls delayed vertex advection and determines when vertices reset to their seeding positions. Elapsed time further regulates advection delays and resets, as shown in Equation 6. As described in Section 4.5, each vertex ($\mathbf{x}_{i,j}$) starts at its seeding position ($\mathbf{s}_j$) before being advected. Vertices with the same i are released simultaneously once the elapsed time (i.e., time after t_{start}) exceeds their release time (t_{rel}). They are advected until the time since release ($t_{\text{start}} - t_{\text{rel}}$) surpasses $t_{\max}$. As t_{start} increases, the lifetime of a vertex $\ell(\mathbf{x}_{i,j})$ is constrained to the interval $(0, 1]$ by applying a floating-point modulo operation over multiple cardiac cycles:

$$t_{\max} = M \cdot t_{\text{col}}, \tag{4}$$

$$t_{\text{rel}} = i \cdot t_{\text{col}}, \tag{5}$$

$$\ell(\mathbf{x}_{i,j}) = 1 - \left(\frac{t_{\text{start}} - t_{\text{rel}}}{t_{\max}} \bmod 1 \right). \tag{6}$$

The **face shader** calculates each face's normal, area, and α_{shape}, along with the longest edge length for our enhanced α_{shape} calculation.

The **mesh vertex shader** converts per-face values to per-vertex values. It assigns α_{shape} and area as the minimum of adjacent cells, averages neighboring cell normals for the vertex normal, and computes $\alpha_{\text{curvature}}$. When a ray intersects the surface, the closest-hit shader determines shading and surface properties. For smoke surface intersections, α_{density} is derived from triangle area and ray angle. The final opacity and color are then passed to the ray generation shader.

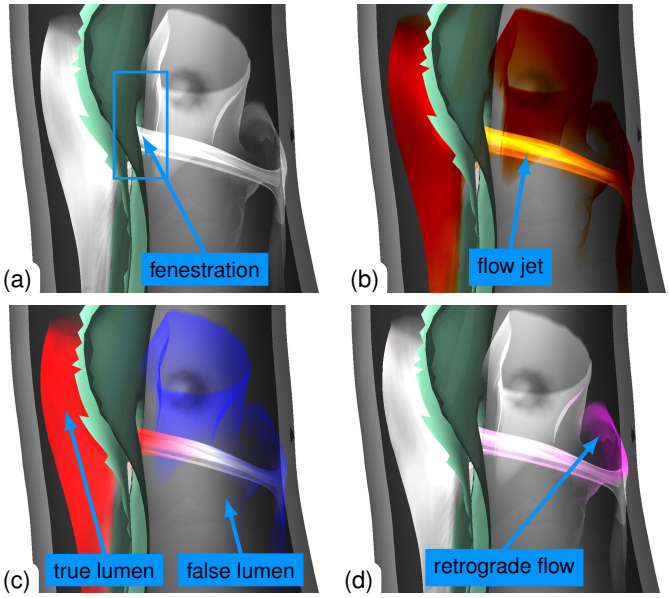

Fig. 4: Demonstration of color mappings on the same streak surface. (a) shows a solid white color. (b) utilizes a heated-body color scale for flow velocity. (c) displays a diverging red-blue scale for luminal origin. (d) applies a monochrome scale to highlight retrograde flow in magenta.

5 Evaluation

The design of our evaluation was developed in collaboration with radiologists experienced in aortic dissection, fluid simulation specialists, and visualization specialists. The evaluation was conducted through an online questionnaire to investigate the flow visualizations' usefulness to both medical experts and researchers, and to gather detailed feedback. Participants (n=14, with 5 being coauthors) included medical professionals (n=4), fluid simulation experts (n=6), and visualization specialists (n=4), most with extensive experience in cardiovascular disease research, particularly aortic dissection.

The online questionnaire included videos of the three visualization techniques for participants to review, rate, and provide subjective feedback on. Participants were not able to interact with our application, but the videos accurately represent the interactive visualizations and their frame rates. This video-based approach was chosen to enable participation from as many members of the three specialized expert groups as possible. For each visualization method, a preset of visualization parameters was developed in collaboration with domain experts to produce informative representations. Consequently, the following parameters remain consistent across all videos in the questionnaire:

- Streaklines with halos: line width, halo width.
- Transparent streaklines: line width, fade out.
- Smoke surfaces: α parameters.

The presented regions of the datasets in the videos, as well as the location and size of seeding structures, were also chosen in collaboration with the same experts. The seeding structure location remains consistent across all three techniques within each video scenario, while the seeding structure type is selected based on the specific flow visualization technique being demonstrated. All evaluation videos, along with a live exploration session, are provided in the supplemental material.

Throughout the questionnaire, a total of nine different visualization scenarios were presented. Each scenario included a video demonstrating the three flow visualization techniques (Figure 1), a brief description of the presented structures and visualizations, and two slice views of the relevant CT data for medical professionals' reference. The videos could be viewed in full-screen, paused, rewound, and replayed as many times as participants wished, allowing for detailed inspection and comparison. After presenting the flow visualization techniques in a synchronized view for each scenario, participants were asked a series of questions.

We asked participants to answer a total of 47 questions. Of these, 33 questions were presented on a 5-point Likert scale, each repeated for all three techniques. The remaining 14 were open-ended questions, allowing participants to explain their answers or provide feedback.

Participants were asked to rate the three flow visualization techniques according to the following aspects using Likert scales:

- Confidence: Highly unconfident, Unconfident, Neutral, Confident, Highly confident
- Visual clutter: None, Slight, Moderate, High, Overwhelming
- Lifelikeness: Highly not lifelike, Not lifelike, Neutral, Lifelike, Highly lifelike
- Preference: Highly unpreferable, Unpreferable, Neutral, Preferable, Highly preferable
- Work impact: Negative impact, Slightly negative impact, No impact, Slightly positive impact, Positive impact

In addition to rating these five aspects, participants were asked whether specific flow phenomena were visible in the visualizations. Unlike the opinion-based ratings, participants' responses to these visibility questions can be assessed for accuracy.

Table 1 presents the aggregated evaluation results. Each cell shows the rating of a specific aspect by a particular group as mean with standard deviation, color-coded to reflect the score. Rows correspond to participant groups, while columns represent the flow visualization techniques. The first five aspects are based on participants' subjective ratings, whereas the remaining five assess their accuracy in identifying flow phenomena. This layout facilitates simultaneous comparison of each aspect across techniques and participant groups. The color scheme provides a visual overview: red indicates poor, yellow represents neutral, and green signifies excellent ratings. Additionally, detailed plots of the evaluation results are provided in the supplemental material.

Table 1: Evaluation results of visualization techniques (columns) by participant group (rows) and visualization aspect (blocks). Each cell shows mean with standard deviation, color-coded from poor (red) through neutral (yellow) to excellent (green). The first five aspects assess subjective ratings, while the remaining five evaluate accuracy in identifying flow phenomena. The final two blocks compare changes in impingement zone (IZ) location and size without (I) and with (II) pressure-based color mapping. For visual clutter assessment, lower values are better.

	HL	TS	SS	HL	TS	SS
	1. Confidence			2. Visual clutter		
MED	3.50±0.41	3.53±0.36	3.64±0.64	3.38±1.01	1.94±0.85	1.63±0.60
CFD	3.56±0.19	3.69±0.61	3.74±0.52	2.96±0.89	1.96±0.19	1.54±0.43
VIS	3.75±0.89	3.61±0.55	3.83±0.28	3.50±0.35	2.50±0.71	1.81±0.38
	3. Lifelikeness			4. Preference		
MED	2.50±0.35	3.19±0.43	3.69±0.72	3.18±0.49	3.57±0.30	3.76±0.92
CFD	2.79±0.37	3.38±0.34	3.88±0.38	3.05±0.64	3.50±0.24	3.61±0.67
VIS	2.56±0.77	3.00±0.61	3.69±0.47	3.22±0.30	3.41±0.30	3.60±0.50
	5. Work impact			6. Entry tear flow		
MED	3.94±0.83	4.06±0.88	4.06±0.97	4.00±0.82	3.50±1.00	3.50±1.73
CFD	3.13±0.41	3.42±0.52	3.58±0.56	3.50±1.38	3.83±0.75	3.83±0.75
VIS	3.38±0.43	3.44±0.38	3.75±0.29	3.75±1.26	3.25±0.96	3.50±1.29
	7. Flow jet origin			8. Drainage pattern		
MED	4.50±1.00	4.50±1.00	4.50±1.00	4.50±1.00	4.00±0.96	4.00±0.96
CFD	4.33±1.63	4.33±1.63	4.33±1.63	3.17±1.33	2.83±1.33	2.67±1.51
VIS	4.50±1.00	4.50±1.00	4.50±1.00	4.00±0.82	3.75±1.26	3.25±1.50
	9. IZ change I			10. IZ change II		
MED	3.25±0.50	3.25±0.50	3.00±0.00	3.75±0.96	3.75±0.96	3.75±0.96
CFD	3.67±0.52	3.50±0.55	3.33±0.82	4.17±1.60	4.17±1.60	4.17±1.60
VIS	3.00±1.41	3.00±1.41	2.75±1.26	2.75±0.96	2.75±0.96	2.75±0.96

MED... medical professional
CFD... fluid simulation expert
VIS ... visualization specialist
IZ ... impingement zone
HL ... streaklines with halos
TS ... transparent streaklines
SS ... smoke surfaces

6 Results and Discussion

This section presents the results of our flow visualization for aortic dissections and how it compared to more common techniques. Adaptations to opacity terms reduced artifacts and improved visual fidelity within the vascular setting. Color mappings were used to encode the flow attributes velocity, direction, and lumen-of-origin, enhancing interpretability and differentiation of flow patterns between lumina.

6.1 Sparse Voxel Grid

The sparse voxel grid structure was tested on three datasets obtained from simulation results in tetrahedral mesh format. Advection results from the original mesh were compared to voxel grids of varying resolutions. A voxel size of 1 mm provided a good balance, showing strong agreement with the original mesh while keeping memory usage manageable. Each of the 40 timesteps was individually converted to a structured voxel grid, resulting in sizes of 1.89 gigabyte (GB) (dataset 1), 13.45 GB (dataset 2), and 4.04 GB (dataset 3). The sparse voxel representation was then applied with a chunk size of 4, where each chunk contains 4^3 voxels. This reduced dataset 1 to 0.43 GB (22.8%), dataset 2 to 1.18 GB (8.8%), and dataset 3 to 0.82 GB (20.4%).

6.2 Seeding

The streak surfaces used for flow visualization are seeded using a closed polygonal seeding structure. During the exploration of an aortic dissection dataset, users can choose size and location of the seeding structure. The seeding location is defined as a percentage along the luminal centerline, while its size is determined as a percentage of the cross-sectional diameter. Users can interact with the seeding structure by adjusting these two values. Using this technique, the seeding of streak surfaces can be adjusted to the needs of the user. Seeding at the aortic root may reveal supply of branching vessels and potential vortices, as illustrated in Figure 1. Conversely, seeding close before a fenestration can reveal the magnitude of cross-flow between lumina and possible flow jets, as seen in Figure 4. The circular seeding structure encompasses all angles within the luminal cross-section, ensuring comprehensive coverage of the flow dynamics. In contrast, a line seeding structure requires selecting both a specific location and rotation, which can lead to missed flow patterns—especially through fenestrations or branching vessels. By covering the lumen entirely, the circular seeding structure reduces this risk and provides a more complete representation of the blood flow.

6.3 Evaluation

Subsequently, we compare smoke surfaces to streak lines (see Section 4.4) computed identically but rendered differently. The first augmentation of streaklines lacks opacity modulation, instead using depth-dependent halos [41] to reduce clutter. The second augmentation uses transparent streaklines with an opacity gradient along each line.

6.3.1 Subjective Rating

Participants generally rated their confidence in understanding aortic flow as "Moderate to Confident" (Table 1, block 1). Across all groups, smoke surfaces achieved the highest confidence ratings, though by a small margin. On average, both streakline techniques performed similarly. This demonstrates that all three techniques support task (T1).

Streaklines with halos exhibited the highest visual clutter, rated as "Moderate" by CFD simulation specialists and "Moderate to High" by the other two groups (Table 1, block 2). Multiple participants specifically mentioned that the clutter was distracting and made the flow harder to discern. Transparent streaklines performed better, receiving an average clutter rating of "Moderate." However, some participants felt they were sometimes too faint for proper clinical assessment. Smoke surfaces generated the least clutter, rated as "Slight to None" by all groups. Participants generally appreciated the reduced clutter and smooth appearance of smoke surfaces, with multiple stating they were the most visually appealing and lifelike. A radiologist commented that smoke surfaces performed best at visualizing flow, while two others highlighted their resemblance to intravascular contrast agent injections used in interventional procedures. One participant noted that artifacts from the streakline structure were visible with streaklines with halos, while they were less noticeable in transparent streaklines and absent in smoke surfaces. This is illustrated in Figure 5, where streaklines with halos exhibit spurious connections between lines in the true and false lumen. While the same connections are present in transparent streaklines, they are less noticeable. Only smoke surfaces effectively conceal these false connections, reducing clutter and eliminating artifacts.

When evaluating realism, smoke surfaces were rated "Lifelike" by all groups (Table 1, block 3). Transparent streaklines were rated "Neutral" and streaklines with halos between "Not lifelike" and "Neutral."

Transparent streaklines were generally preferred over streaklines with halos, with smoke surfaces being slightly more favored overall (Table 1, block 4). Several participants noted that transparent streaklines offered a good compromise between the two techniques, reducing clutter compared to streaklines with halos but sometimes appearing too faint. Multiple participants explained that they preferred the appearance of smoke surfaces but found that streaklines with halos were best for quantifying flow. Consequently, (T2) appears to be supported by all techniques, with streaklines with halos providing the best quantification.

The potential impact of the flow visualization techniques varied among participant groups (Table 1, block 5). CFD simulation and visualization specialists generally rated all techniques as having "No impact" or only a "Slight positive impact" on their work. In contrast, medical professionals consistently rated all techniques as having a "Slight positive impact". Across all groups, smoke surfaces were considered to have the most significant positive impact.

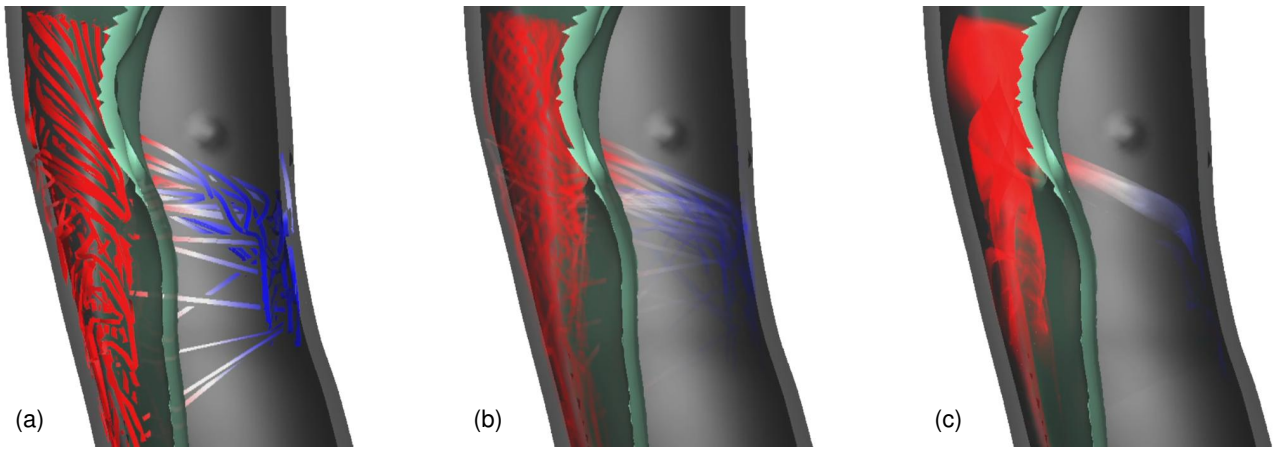

Fig. 5: Freeze-frame from an evaluation video showing flow through a fenestration. Streaklines with halos (a), transparent streaklines (b), and smoke surfaces (c), all using lumen-of-origin color mapping with true lumen in red and false lumen in blue. Seeding location, structure length, color mapping, and viewing direction are synchronized. Dispersed flow fades more rapidly in the smoke surface visualization than in either streakline variant.

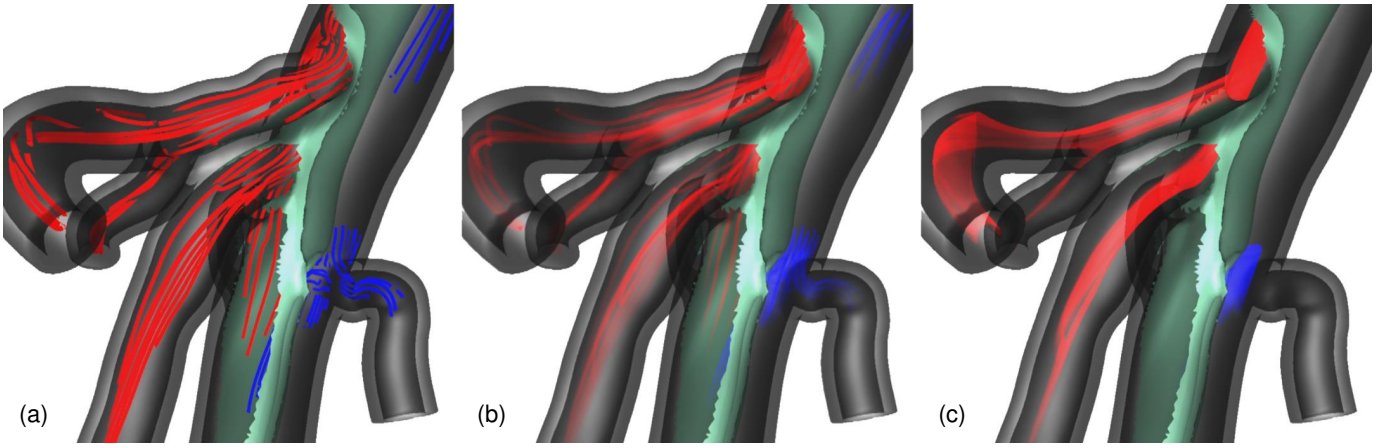

Fig. 6: Freeze-frame from an evaluation video showing flow into abdominal aorta branches. Streaklines with halos (a), transparent streaklines (b), and smoke surfaces (c), all using lumen-of-origin color mapping with true lumen in red and false lumen in blue. Seeding location, structure length, color mapping, and viewing direction are synchronized. Flow in the false lumen (top right) appears less prominent in the smoke surface visualization due to faster opacity fading.

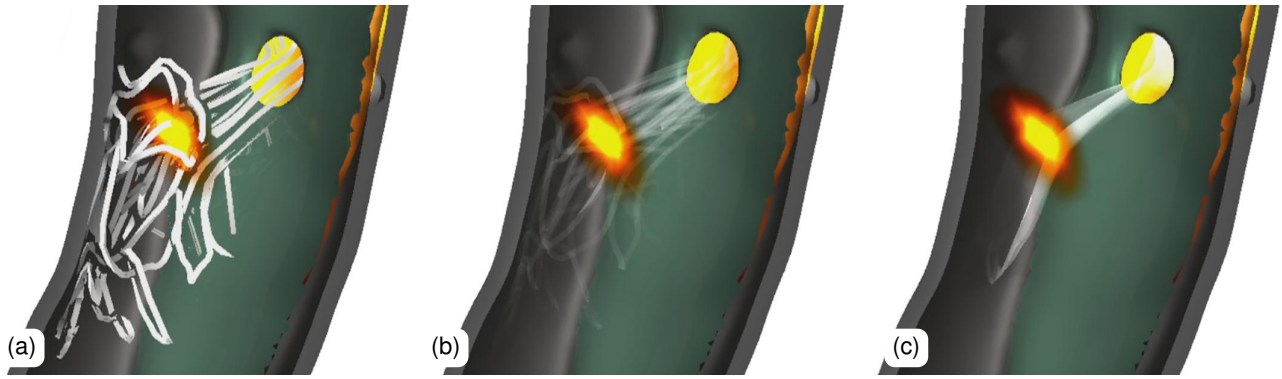

Fig. 7: Freeze-frame from a demonstration video used in the evaluation, showing flow through a fenestration in the dissection flap. Streaklines with halos (a), transparent streaklines (b), and smoke surfaces (c), all displayed with solid white color and pressure-based color mapping overlaid on the outer vessel wall. Seeding location, structure length, color mapping, and viewing direction are synchronized.

6.3.2 Assessment of Flow

Participants were asked to determine whether retrograde flow through the entry tear was visible using the different flow visualization techniques (Table 1, block 6). They were shown a video of the visualization in Figure 1. CFD simulation specialists assessed the flow most accurately with transparent streaklines and smoke surfaces, while medical and visualization specialists were most accurate with streaklines with halos. Overall, streaklines with halos were the most effective, followed closely by smoke surfaces, with transparent streaklines performing the least accurately. Participants explain, that streaklines with halos give the strongest signal for the color map, but smoke surfaces show retrograde flow well. All three techniques provide a visualization to support (T3), but transparent streaklines are unpreferable for this task.

All participant groups were able to accurately assess the origin of a flow jet through a fenestration in the dissection flap, based on the visualization in Figure 5. All three techniques performed equally well, achieving the same score (Table 1, block 7).

Next, participants assessed whether a branching vessel was supplied by the true lumen (Table 1, block 8). Medical professionals accurately determined this using any technique but felt most confident with streaklines with halos. In contrast, visualization and CFD simulation specialists were highly uncertain when using transparent streaklines and smoke surfaces. While visualization specialists correctly identified the contribution of the true lumen, CFD simulation specialists occasionally misidentified the flow. Although medical professionals could assess flow accurately using any technique, only streaklines with halos consistently supported (T4) across all participant groups.

Some participants noted that streaklines with halos provided more detail in certain cases. One participant explained that they conveyed the most information about the flow field, while another mentioned that streaklines with halos performed best for identifying details in thinner vessels but suffered from occlusion and clutter in larger lumina. Figure 6 illustrates the visualization used to assess the luminal drainage pattern. Among the three techniques, streaklines with halos most prominently highlight the flow into the left renal artery (right side of the image). While transparent streaklines still reveal the vessel's supply, smoke surfaces fail to depict this phenomenon effectively.

Participants were asked to determine whether the impingement zone caused by a flow jet changed in position and size over time. Initially, they were shown a visualization without any color mappings. No group felt confident identifying these changes with any technique (Table 1, block 9). On average, streaklines with halos performed best, but confidence remained within the range of "Uncertain" to "Probably yes". Next, a pressure encoding on the outer vessel wall was added, as illustrated in Figure 7. With this enhancement, all three techniques performed equally well across participant groups (Table 1, block 10). While accuracy improved for medical professionals and significantly for CFD simulation specialists, visualization specialists' accuracy declined for both streakline-based techniques.

All techniques successfully visualized the flow jet, supporting (T5). Without pressure color mapping, only the streakline-based techniques were able to support (T6). With the color mapping, smoke surfaces also supported (T6). While the color mapping generally improved accuracy, it caused some confusion among visualization specialists.

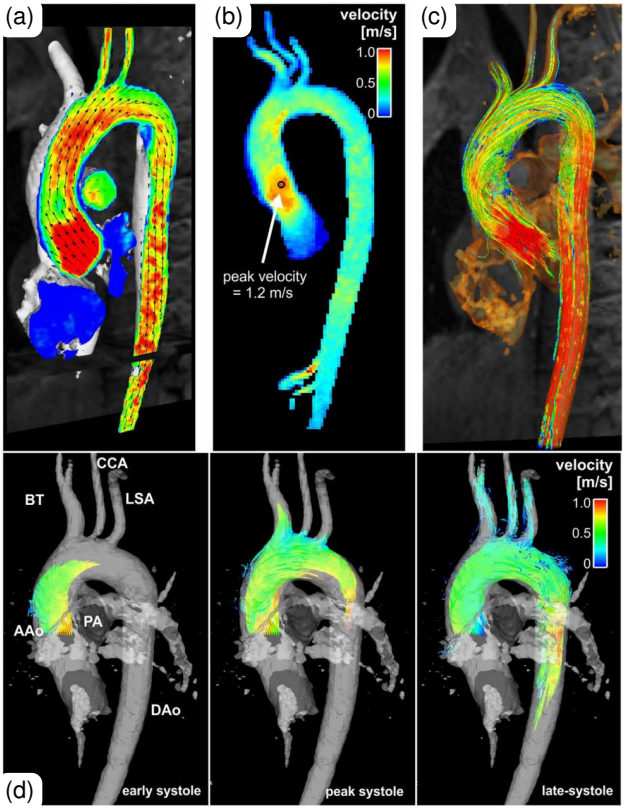

Fig. 8: Visualization of aortic flow based on 4D flow MRI in clinical practice. Image from Dyverfeldt et al. [44], licensed under CC-BY.

Figure 8 demonstrates flow visualization techniques used for 4D flow MRI in clinical practice. Subfigures (a), (b), and (c) depict methods that do not incorporate time-varying flow data, each with notable limitations: (a) is restricted to a single slice, (b) lacks flow trajectory information, and (c) suffers from clutter and occlusion. Subfigure (d) demonstrates pathlines, which capture the temporal aspect of flow but still experience clutter and occlusion. Additionally, pathlines do not provide the realistic and dynamic representation that streaklines offer.

The three techniques discussed in this work convey more information while addressing occlusion and clutter to varying degrees. Although their effectiveness at reducing clutter differs, they provide a more intuitive and comprehensive visualization of aortic dissection hemodynamics compared to current clinical methods. This is supported by a statement from one medical professional, who noted that the information gained through our visualization system is prognostically relevant and potentially informative for the development of future treatments.

6.4 Limitations

Smoke surfaces were effectively used to visualize flow in aortic dissection, but several limitations emerged during testing. Despite efforts to conceal artifacts where flow diverges, minor issues inherent to streak surfaces without remeshing persist, though they were only briefly visible when a surface passed through a fenestration. Refining opacity calculations could reduce artifacts but risks overly diminishing overall visibility. The circular seeding structure often requires user adjustments for size and placement, particularly when examining flow near complex geometries such as fenestrations. This is due to the significant differences between flow near the vessel wall and flow at the center of the lumen. Uniform seeding across the entire cross-section could help to capture all flow features. While interactive adjustments allow for exploratory investigation, simultaneous seeding at both the wall and center is not currently supported. Advection performance varies with the number of streak surface vertices. Larger surfaces can cause overlapping transparent layers, slowing rendering and limiting surface size and resolution to maintain interactive frame rates.

We did not control for visibility and geometric content between the three flow visualization techniques. Interactive adjustment of visualization parameters was not available to participants during the evaluation. While the presets were developed in collaboration with domain experts to ensure clinical relevance, the interactive seeding component—which supports exploratory analysis—was not evaluated as part of the study.

7 Conclusion and Future Work

This work aimed to develop smoke-like visualizations of aortic dissection hemodynamics that enhance visualization clarity, information density, and intuitive blood flow analysis. We compared their effectiveness to more established flow visualization techniques. We implemented a streak surface technique by von Funck et al. [12], selected for its capacity to generate interactive, smoke-like flow visualizations, and adapted it to address the unique physiological complexities of aortic dissection. For comparative evaluation, we also implemented streaklines with depth-dependent halos and transparent streaklines. To establish a comprehensive focus-and-context representation, all techniques display blood flow together with vessel morphology.

We conducted a user study with 14 participants who evaluated each technique regarding confidence in flow understanding, visual clutter, lifelikeness, preference, and potential work impact. Results were analyzed separately for three expert groups, revealing domain-specific preferences and interpretation accuracy. Smoke surfaces demonstrated the least visual clutter and most appealing appearance, with medical professionals noting their similarity to interventional methods used in clinical practice. Participants noted that transparent streaklines and smoke surfaces dissipated more quickly, while streaklines with halos performed better for identifying drainage patterns and flow in thin vessels. Despite experiencing the highest visual clutter and being rated as the least lifelike and least preferred technique, streaklines with halos appeared particularly useful for flow quantification. Transparent streaklines were generally perceived as offering a balanced compromise between smoke surfaces and streaklines with halos.

All three flow visualization techniques support the visualization tasks outlined in Section 3, albeit to varying degrees. Streaklines with halos performed best for assessing flow in UC 1, while all techniques supported UC 3 equally well when explicit pressure mapping was added to the outer vessel wall. Transparent streaklines, while ranking second in most aspects, did not excel in any particular task, making them less favorable overall. An interesting finding of our study was that subjective preference of participants did not coincide with accuracy, as they preferred smoke surfaces but demonstrated higher accuracy with streaklines with halos. Due to such contrasting findings and the overall similar scores, no single technique proved most effective. Therefore, a hybrid visualization system incorporating both streaklines with halos and smoke surfaces would likely offer the most effective solution.

This work marks the first attempt to enhance aortic dissection flow visualizations using a smoke-like technique, leaving room for refinement or exploration of alternative methods. While our circular seeding structure samples at a relative distance from the cross-section center, alternative structures, such as spirals or multiple rings, could provide more even sampling. However, overlapping streak surfaces from such designs may reduce clarity. One future avenue is a more intuitive method for interactively adjusting the size and location of the seeding structure to expand exploratory analysis.

While we adapted the opacity calculations of von Funck et al. [12] to hide artifacts through the flap, we could implement an intersection test between the smoke surface and vessel wall to eliminate false connections in the surface. Beyond streak surfaces, particle- and volume-based techniques could be explored as alternative visualization approaches. Adapting particle methods demonstrated by de Hoon et al. [23] for aortic hemodynamics to dissection datasets is another promising direction.

There are also several avenues to extend our user study. Interactive adjustment of both seeding and visualization parameters would provide valuable insights into user preferences. Another important aspect is providing experts with the possibility to directly interact with our visualization system for interactive exploration, which would better evaluate the practical utility and usability of the proposed techniques.

References

[1] Maya Landenhed, Gunnar Engström, Anders Gottsäter, Michael P. Caulfield, Bo Hedblad, Christopher Newton-Cheh, Olle Melander, and J. Gustav Smith. Risk profiles for aortic dissection and ruptured or surgically treated aneurysms: A prospective cohort study. *Journal of the American Heart Association*, 4(1), 2015. 1

[2] Maximilian Wundram, Volkmar Falk, Jaime-Jürgen Eulert-Grehn, Hermann Herbst, Jana Thurau, Bernd A. Leidel, Eva Göncz, Wolfgang Bauer, Helmut Habazettl, and Stephan Kurz. Incidence of acute type A aortic dissection in emergency departments. *Scientific Reports*, 10(1):7434, May 2020. 1

[3] Kathrin Bäumler, Vijay Vedula, Anna Sailer, Jongmin Seo, Peter Chiu, Gabriel Mistelbauer, Frandics Chan, Michael Fischbein, Alison Marsden, and Dominik Fleischmann. Fluid–structure interaction simulations of patient-specific aortic dissection. *Biomechanics and Modeling in Mechanobiology*, 19(5):1607–28, 2020. 1, 3

[4] Domenico Spinelli, Filippo Benedetto, Rocco Donato, Gabriele Piffaretti, Massimiliano Marrocco-Trischitta, Himanshu Patel, Kim Eagle, and Santi Trimarchi. Current evidence in predictors of aortic growth and events in acute type B aortic dissection. *Journal of Vascular Surgery*, 68(6):1925–35, 2018. 1

[5] Jin Wook Chung, Christopher Elkins, Toyohiko Sakai, Noriyuki Kato, Thomas Vestring, Charles Semba, Suzanne Slonim, and Michael Dake. True-lumen collapse in aortic dissection: part I. Evaluation of causative factors in phantoms with pulsatile flow. *Radiology*, 214(1):87–98, 2000. 2

[6] Jin Wook Chung, Christopher Elkins, Toyohiko Sakai, Noriyuki Kato, Thomas Vestring, Charles P. Semba, Suzanne M. Slonim, and Michael D. Dake. True-lumen collapse in aortic dissection: part II. Evaluation of treatment methods in phantoms with pulsatile flow. *Radiology*, 214(1):99–106, 2000. 2

[7] Ramon Berguer, Juan Parodi, Marty Schlicht, and Khalil Khanafer. Experimental and clinical evidence supporting septectomy in the primary treatment of acute type B thoracic aortic dissection. *Annals of Vascular Surgery*, 29(2):167–73, 2015. 2

[8] Thomas T. Tsai, Marty S. Schlicht, Khalil Khanafer, Joseph L. Bull, Doug T. Valassis, David M. Williams, Ramon Berguer, and Kim A. Eagle. Tear size and location impacts false lumen pressure in an ex vivo model of chronic type B aortic dissection. *Journal of Vascular Surgery*, 47(4):844–51, 2008. 2

[9] Barry Doyle and Paul Norman. Computational biomechanics in thoracic aortic dissection: Today's approaches and tomorrow's opportunities. *Annals of Biomedical Engineering*, 44(1):71–83, 2015. 2

[10] Anna Sailer, Patricia Nelemans, Trevor Hastie, Anne Chin, Mark Huininga, Peter Chiu, Michael Fischbein, Michael Dake, D. Miller, Geert Schurink, and Dominik Fleischmann. Prognostic significance of early aortic remodeling in acute uncomplicated type B aortic dissection and intramural hematoma. *The Journal of Thoracic and Cardiovascular Surgery*, 154(4):1192–200, 2017. 2

[11] Aaron Schroeder, Kai Ostendorf, Kathrin Bäumler, Domenico Mastrodicasa, Veit Sandfort, Dominik Fleischmann, Bernhard Preim, and Gabriel Mistelbauer. Advanced visualization of aortic dissection anatomy and hemodynamics. *Computers & Graphics*, 124:104060, 2024. 2, 3, 5

[12] W. von Funck, T. Weinkauf, H. Theisel, and H.-P. Seidel. Smoke surfaces: An interactive flow visualization technique inspired by real-world flow experiments. *IEEE Transactions on Visualization and Computer Graphics*, 14(6):1396–1403, 2008. 2, 3, 4, 5, 9

[13] Yusman Azimi Yusoff, Farhan Mohamad, Mohd Shahrizal Sunar, and Ali Selamat. *Flow Visualization Techniques: A Review*, pages 527–538. Springer International Publishing, 2016. 2

[14] Steffen Oeltze-Jafra, Monique Meuschke, Mathias Neugebauer, Sylvia Saalfeld, Kai Lawonn, Gabor Janiga, Hans-Christian Hege, Stefan Zachow, and Bernhard Preim. Generation and visual exploration of medical flow data: Survey, research trends, and future challenges. *Computer Graphics Forum*, 38, March 2018. 2

[15] Benjamin Köhler, Matthias Grothoff, Matthias Gutberlet, and Bernhard Preim. Bloodline: A system for the guided analysis of cardiac 4D PC-MRI data. *Computers & Graphics*, 82:32–43, 2019. 2

[16] Pepe Eulzer, Monique Meuschke, Carsten M Klingner, and Kai Lawonn. Visualizing carotid blood flow simulations for stroke prevention. *Computer Graphics Forum*, 40(3):435–446, 2021. 2

[17] Kai Lawonn, Sylvia Glaßer, Anna Vilanova, Bernhard Preim, and Tobias Isenberg. Occlusion-free blood flow animation with wall thickness visualization. *IEEE Transactions on Visualization and Computer Graphics*, 22(1):728–737, 2016. 2

[18] Benjamin Behrendt, Wito Engelke, Philipp Berg, Oliver Beuing, Ingrid Hotz, Bernhard Preim, and Sylvia Saalfeld. Visual exploration of intracranial aneurysm blood flow adapted to the clinical researcher. In *Eurographics – Dirk Bartz Prize*, 2021. 2

[19] Kai Ostendorf, Domenico Mastrodicasa, Kathrin Bäumler, Marina Codari, Valery Turner, Martin J. Willemink, Dominik Fleischmann, Bernhard Preim, and Gabriel Mistelbauer. Shading Style Assessment for Vessel Wall and Lumen Visualization. The Eurographics Association, 2021. 2

[20] J.J. van Wijk. Rendering surface-particles. In *Proc. of IEEE Visualization*, pages 54–61, 1992. 2

[21] Thorsten Holtkämper. Real-time gaseous phenomena: a phenomenological approach to interactive smoke and steam. In *Proc. of International Conference on Computer Graphics, Virtual Reality, Visualisation and Interaction in Africa*, AFRIGRAPH '03, pages 25–30. Association for Computing Machinery, 2003. 2

[22] Jens Krueger and Ruediger Westermann. GPU Simulation and Rendering of Volumetric Effects for Computer Games and Virtual Environments. *Computer Graphics Forum*, 24(3):685–694, 2005. 2

[23] Niels deHoon, Kai Lawonn, Andrei C. Jalba, Elmar Eisemann, and Anna Vilanova. InkVis: A High-Particle-Count Approach for Visualization of Phase-Contrast Magnetic Resonance Imaging Data. *Eurographics Workshop on Visual Computing for Biology and Medicine*, 2019. 2, 3, 9

[24] J.J. van Wijk. Implicit stream surfaces. In *Proc. of IEEE Visualization*, pages 245–252, 1993. 2

[25] G. Scheuermann, T. Bobach, H. Hagen, K. Mahrous, B. Hamann, K.I. Joy, and W. Kollmann. A tetrahedra-based stream surface algorithm. In *Proc. of IEEE Visualization*, pages 151–553, 2001. 2

[26] Christoph Garth, Xavier Tricoche, Tobias Salzbrunn, Tom Bobach, and Gerik Scheuermann. Surface techniques for vortex visualization. In *Proc. of Eurographics / IEEE VGTC Symposium on Visualization*, 2004. 2

[27] Tobias Schafhitzel, Eduardo Tejada, Daniel Weiskopf, and Thomas Ertl. Point-based stream surfaces and path surfaces. In *Proc. of Graphics Interface*, pages 289–296, 2007. 2

[28] Kai Bürger, Florian Ferstl, Holger Theisel, and Rüdiger Westermann. Interactive Streak Surface Visualization on the GPU. *IEEE Transactions on Visualization and Computer Graphics*, 15(6):1259–1266, 2009. 2

[29] Florian Ferstl, Kai Burger, Holger Theisel, and Rudiger Westermann. Interactive separating streak surfaces. *IEEE Transactions on Visualization and Computer Graphics*, 16(6):1569–1577, 2010. 2

[30] Mathias Hummel, Christoph Garth, Bernd Hamann, Hans Hagen, and Kenneth I. Joy. Iris: Illustrative rendering for integral surfaces. *IEEE Transactions on Visualization and Computer Graphics*, 16(6):1319–1328, 2010. 2

[31] Marwin Schindler, Aleksandr Amirkhanov, and Renata Georgia Raidou. Smoke Surfaces of 4D Biological Dynamical Systems. In *Proc. of Eurographics Workshop on Visual Computing for Biology and Medicine*, 2023. 2

[32] Joshua Schpok, Joseph Simons, David S. Ebert, and Charles Hansen. A real-time cloud modeling, rendering, and animation system. In *Proc. of ACM SIGGRAPH/Eurographics Symposium on Computer Animation*, pages 160–166, 2003. 3

[33] Kun Zhou, Zhong Ren, Stephen Lin, Hujun Bao, Baining Guo, and Heung-Yeung Shum. Real-time smoke rendering using compensated ray marching. *ACM Transactions on Graphics (TOG)*, 27(3):1–12, 2008. 3

[34] Nelson Max, Becker G., and Roger Crawfis. Flow volumes for interactive vector field visualization. In *Proc. of IEEE Visualization*, pages 19–24, November 1993. 3

[35] Will Schroeder, Kenneth M. Martin, and William E. Lorensen. *The visualization toolkit (2nd ed.): an object-oriented approach to 3D graphics*. Prentice-Hall, Inc., USA, 1998. 3

[36] Jane Wilhelms and Allen Van Gelder. Octrees for faster isosurface generation. *ACM Trans. Graph.*, 11(3):201–227, 1992. 3

[37] Nathan Andrysco and Xavier Tricoche. Matrix trees. *Computer Graphics Forum*, 29(3):963–972, 2010. 3

[38] Abhishek Yenpure, Sudhanshu Sane, Roba Binyahib, David Pugmire, Christoph Garth, and Hank Childs. State-of-the-Art Report on Optimizing Particle Advection Performance. *Computer Graphics Forum*, 2023. 3

[39] David Marlevi, Julio A. Sotelo, Ross Grogan-Kaylor, Yunus Ahmed, Sergio Uribe, Himanshu J. Patel, Elazer R. Edelman, David A. Nordsletten, and Nicholas S. Burris. False lumen pressure estimation in type B aortic dissection using 4D flow cardiovascular magnetic resonance: comparisons

with aortic growth. *Journal of Cardiovascular Magnetic Resonance*, 23(1), 2021. 3

[40] George G. Hartnell and Julia Gates. Aortic fenestration: A why, when, and how-to guide. *RadioGraphics*, 25(1):175–189, 2005. 3

[41] Maarten H. Everts, Henk Bekker, Jos B. T. M. Roerdink, and Tobias Isenberg. Depth-dependent halos: Illustrative rendering of dense line data. *IEEE Transactions on Visualization and Computer Graphics*, 15(6):1299—-306, 2009. 3, 4, 7

[42] R. Gasteiger, M. Neugebauer, C. Kubisch, and B. Preim. Adapted Surface Visualization of Cerebral Aneurysms with Embedded Blood Flow Information. In *Proc. of the Eurographics Workshop on Visual Computing for Biology and Medicine*, 2010. 3

[43] The Khronos® Group Inc J. Vulkan: Cross platform 3D graphics, 2022. https://www.vulkan.org/. 5

[44] Petter Dyverfeldt, Malenka Bissell, Alex J. Barker, Ann F. Bolger, Carl-Johan Carlhäll, Tino Ebbers, Christopher J. Francios, Alex Frydrychowicz, Julia Geiger, Daniel Giese, Michael D. Hope, Philip J. Kilner, Sebastian Kozerke, Saul Myerson, Stefan Neubauer, Oliver Wieben, and Michael Markl. 4d flow cardiovascular magnetic resonance consensus statement. *Journal of Cardiovascular Magnetic Resonance*, 17(1):72, 2015. 9